

Doppler broadening of annihilation radiation measurements on $3d$ and $4f$ ferromagnets using polarized positrons

A. Kawasuso,* M. Maekawa, Y. Fukaya, A. Yabuuchi, and I. Mochizuki

Advanced Science Research Center, Japan Atomic Energy Agency, 1233 Watanuki, Takasaki, Gunma JP-370-1292, Japan

(Received 20 October 2011; published 23 January 2012)

We measured the Doppler broadening of annihilation radiation (DBAR) spectra of $3d$ (Fe, Co, and Ni) and $4f$ (Gd, Tb, and Dy) ferromagnets under a magnetic field by using spin-polarized positrons from a ^{68}Ge - ^{68}Ga source. The results showed that the DBAR spectra of these metals have notably different magnetic-field dependences. The differences among Fe, Co, and Ni reflect that the upper minority spin bands of Fe and Co are nearly empty while those of Ni are still mostly occupied. For the rare-earth metals instead of the inner $4f$ electrons, $5d$ electrons that mediate the exchange interaction of the $4f$ electrons are primarily responsible for the magnetic-field effects on the DBAR spectra. Furthermore, the magnetic-field effects on the DBAR spectra of Gd, Tb, and Dy vanished above the Curie temperatures of the magnetic-phase transition for these metals.

DOI: [10.1103/PhysRevB.85.024417](https://doi.org/10.1103/PhysRevB.85.024417)

PACS number(s): 78.70.Bj, 71.60.+z, 75.50.-y

I. INTRODUCTION

The angular correlation of annihilation radiation (ACAR) is one method of positron annihilation spectroscopy (PAS) that provides an electron-momentum distribution. The ACAR method has been used extensively for the study of Fermi-surface topology. By using longitudinally spin-polarized positrons emitted from radioisotopes, polarized band structures of ferromagnets have also been studied.¹⁻¹⁸ Recently, we demonstrated, by using highly spin-polarized positrons from a ^{68}Ge - ^{68}Ga source, that the technique of Doppler broadening of annihilation radiation (DBAR) can also provide knowledge on polarized electrons.¹⁹

Spin-polarized positron annihilation spectroscopy (SP-PAS) has several attractive points. Low-energy spin-polarized positron beams²⁰⁻²³ are useful to study the magnetism and spin-related phenomena occurring at surfaces and interfaces and in thin films. Considering that positrons are trapped by vacancy defects, SP-PAS can also be used in studying vacancy-induced magnetism.²⁴ In this respect, to detect excess electron spins at vacancy defects, positron-annihilation-lifetime measurements using spin-polarized positrons are also an intriguing experiment.

To establish the SP-PAS method as a probe for ferromagnets and spin-related phenomena, further fundamental studies are needed. In our previous work, we found that the amplitudes of the differential DBAR spectra of Fe, Co, Ni, and Gd are related to their electron polarizations. However, we observed no major differences in their spectral shapes that should reflect the different band structures. Since at that time we focused only on the change in the DBAR spectra upon field reversal, detailed changes of the spectral shapes depending on the magnetic field would have been overlooked. Here, to find structures of DBAR spectra reflecting polarized electron states, we investigated magnetic-field dependences of the DBAR spectra for the above metals. To confirm the effect of the ferromagnetic-phase transition on the DBAR spectra, we also measured the temperature dependences of the DBAR spectra for $4f$ (Gd, Tb, and Dy) ferromagnets having lower Curie temperatures.

II. PRINCIPLE OF SP-DBAR

Before describing the experimental details, we briefly summarize the principle of SP-DBAR. Denoting the majority spin band by \downarrow (magnetic moment is up) and minority spin band by \uparrow (magnetic moment is down), the positron-electron-momentum densities for the i th majority (and minority) spin bands $\rho_i^{\downarrow(\uparrow)}(\mathbf{p})$ are given by

$$\rho_i^{\downarrow(\uparrow)}(\mathbf{p}) = \left| \int e^{-i\mathbf{p}\mathbf{r}} \Psi_+(\mathbf{r}) \Psi_i^{\downarrow(\uparrow)}(\mathbf{r}) \sqrt{\gamma[n_-(\mathbf{r})]} d\mathbf{r} \right|^2, \quad (1)$$

where $\Psi_+(\mathbf{r})$ is the positron wave function, $\Psi_i^{\downarrow(\uparrow)}(\mathbf{r})$ is the electron wave function, and $\gamma[n_-(\mathbf{r})]$ is the enhancement factor.²⁵ The corresponding DBAR spectrum $N_i^{\downarrow(\uparrow)}(p_z)$ is given by the convolution of the apparatus resolution function and the double integral ($dp_x dp_y$) of the above i th electron-positron-momentum density. This expression is valid for a single crystal. For a polycrystal, the DBAR spectrum should be given by a weighted average between those in different momentum axes. In this case, $N_i^{\downarrow(\uparrow)}(p_z)$ is simply replaced with $N_i^{\downarrow(\uparrow)}(p) = \alpha N_i^{\downarrow(\uparrow)}(p_x = p) + \beta N_i^{\downarrow(\uparrow)}(p_y = p) + \gamma N_i^{\downarrow(\uparrow)}(p_z = p)$ with appropriate coefficients.¹³

Two DBAR spectra, $N_+(p_z)$ and $N_-(p_z)$, measured using longitudinally polarized positrons under a magnetic field that is parallel (+) or antiparallel (-) to the positron-polarization vector (see Fig. 1), are given by

$$N_{\pm}(p_z) = \frac{\lambda_S}{4} \sum_{i=1}^{occ} \left[\frac{(1 \pm P) N_i^{\downarrow}(p_z)}{\lambda^{\uparrow}} + \frac{(1 \mp P) N_i^{\uparrow}(p_z)}{\lambda^{\downarrow}} \right], \quad (2)$$

where the summation is over all occupied states; $\lambda_S = 4\pi r_e^2 c$, where r_e is the classical electron radius; P is the longitudinal polarization of positrons; and $\lambda^{\uparrow(\downarrow)}$ is the total annihilation rate of spin-up (spin-down) positrons

$$\lambda^{\uparrow(\downarrow)} = \frac{1}{2} \sum_{i=1}^{occ} [\lambda_S w_i^{\downarrow(\uparrow)} + \lambda_T (w_i^{\downarrow(\uparrow)} + 2w_i^{\uparrow(\downarrow)})]. \quad (3)$$

Here, $\lambda_T = \lambda_S/1115$, and $w_i^{\downarrow(\uparrow)}$ is the overlap integral between the positron and i th majority (minority) spin-band wave

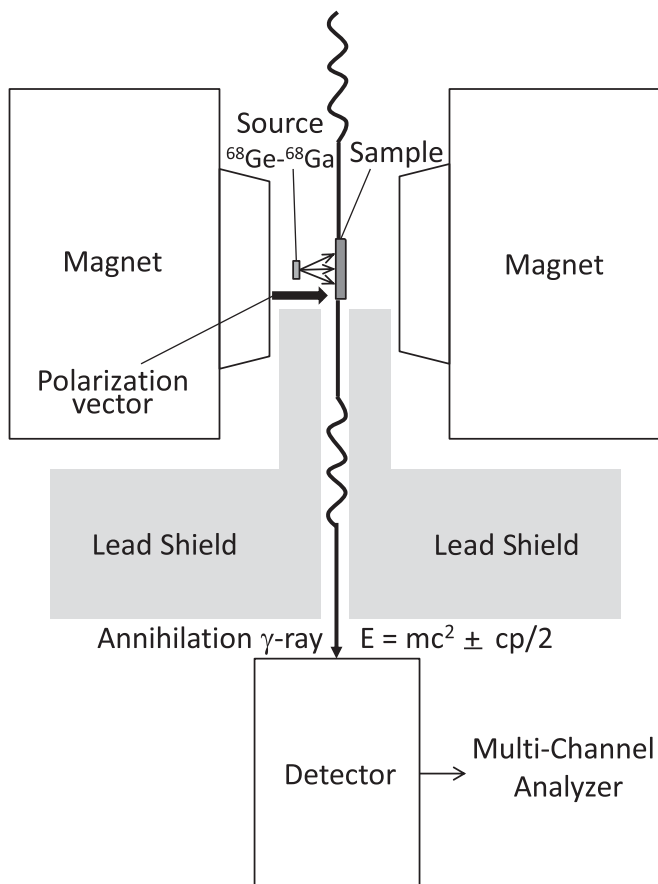


FIG. 1. Experimental setup for spin-polarized DBAR measurements. Positrons emitted from the source are implanted in the sample. Positrons are longitudinally polarized in the direction of the polarization vector. An external magnetic field from -1 T to $+1$ T is applied with the electromagnet. Annihilation radiation from the source is shielded by lead blocks.

functions, equaling $\int_{-\infty}^{+\infty} N_i^{\downarrow(\uparrow)}(p_z) dp_z$. Equation (2) suggests that the DBAR spectrum exhibits the characters of more majority and more minority spin bands under positive and negative fields, respectively. Their difference is given by

$$N_+(p_z) - N_-(p_z) = \frac{\lambda_S P}{2} \sum_{i=1}^{occ} \left[\frac{N_i^{\downarrow}(p_z)}{\lambda^{\uparrow}} - \frac{N_i^{\uparrow}(p_z)}{\lambda^{\downarrow}} \right]. \quad (4)$$

Thus, the differential DBAR spectrum is not a simple summation of partial differential spectra $[N_i^{\downarrow}(p_z) - N_i^{\uparrow}(p_z)]$ unlike the case of the magnetic-Compton-profile measurement. Berko and Mills⁷ proposed that by using field-reversal asymmetry of the three-gamma-annihilation probability, the following relation is obtained:

$$\sum_{i=1}^{occ} [N_i^{\downarrow}(p_z) - N_i^{\uparrow}(p_z)] \propto \Delta N(p_z) + P \frac{\lambda^{\uparrow} - \lambda^{\downarrow}}{\lambda^{\uparrow} + \lambda^{\downarrow}} \Sigma N(p_z) \approx \Delta N(p_z) + P^{3\gamma} \Sigma N(p_z), \quad (5)$$

where $\Delta N(p_z) = N_+(p_z) - N_-(p_z)$, $\Sigma N(p_z) = N_+(p_z) + N_-(p_z)$, and $P^{3\gamma} = (N_+^{3\gamma} - N_-^{3\gamma}) / (N_+^{3\gamma} + N_-^{3\gamma})$. Therefore, either through Eq. (4) or (5), one can extract the components related to magnetic electrons. In the present experiment, to

examine the difference between two DBAR spectra in different field conditions, both experimental and calculated spectra are simply normalized to unity, and differential DBAR spectra are obtained.

III. EXPERIMENTAL METHODS

The samples used in this study were polycrystalline, Fe (4N), Co (5N), Ni (5N), Gd (3N), Tb (3N), and Dy (3N), with dimensions of $10.0 \text{ mm} \times 12.5 \text{ mm} \times 2.0 \text{ mm}$. The samples were mechanically and electrochemically polished and subjected to heat treatment at 1100°C for 2 h in a vacuum. Through the nuclear reaction of $^{69}\text{Ga}(p,2n)^{68}\text{Ge}$ induced by 20-MeV proton irradiation of a GaN substrate ($\phi 8 \text{ mm}$), a positron source ($^{68}\text{Ge}-^{68}\text{Ga}$, 20 MBq) was produced (total fluence: 9×10^{17} protons). Through the magnetic-field dependence of the S parameter related to the self-annihilation of spin-singlet (para-)positronium in $\alpha\text{-SiO}_2$, the longitudinal spin polarization of positrons emitted from the source was determined to be 0.7.²⁶ Basically, in the longitudinal condition, the positron polarization is not lost so much since the polarization vector and magnetic field are parallel (or antiparallel). Nevertheless, depolarization will occur during the thermalization and diffusion processes because of inner magnetic fields.²⁷ To preserve the positron polarization as much as possible, it is important to use a source emitting highly polarized positrons. The samples and the source were placed at the center of a gap in an electromagnet (with a magnetic-field variable up to 1 T), maintaining a distance of 7 mm. The sample temperature was changed from 5 K to 315 K. To detect annihilation radiation from only the samples, the source was shielded by lead blocks. The experimental arrangement is schematically shown in Fig. 1. DBAR spectra were measured by using a high-purity-Ge detector with an energy resolution of 1.4 keV at 511 keV. Here, the photon energy of $E_\gamma = 1 \text{ keV}$ corresponds to an electron momentum of $p = 3.92 \times 10^{-3} m_0 c$ (0.54 a.u.). In each spectrum, more than 10^6 events were accumulated. To compare the differences in spectral shapes under different field conditions in detail, all the spectral area intensities were normalized to unity.

IV. RESULTS AND DISCUSSION

A. Magnetic-field dependence

Figure 2 shows the DBAR spectra of the Fe sample obtained under positive and negative fields ($B = \pm 0.8 \text{ T}$) and the differential spectrum $N_+(p) - N_-(p)$. We call the finite differential spectrum the field-reversal asymmetry. The momentum resolution of DBAR is poorer than that of ACAR. Nevertheless, such field effects are observable. The positive intensity of the differential spectrum at $|p| \gtrsim 5 \times 10^{-3} m_0 c$ was attributed to the enhanced (reduced) annihilation between spin-up positrons and spin-down (spin-up) $3d$ electrons having broader momentum distributions under a positive (negative) field. The negative intensity at $|p| \lesssim 5 \times 10^{-3} m_0 c$ was explained as the relative decrease of low-momentum components. In our previous work, the shapes of the differential spectra $[N_+(p) - N_-(p)]$ for Fe, Co, Ni, and Gd were similar to each other. No further fine structures reflecting

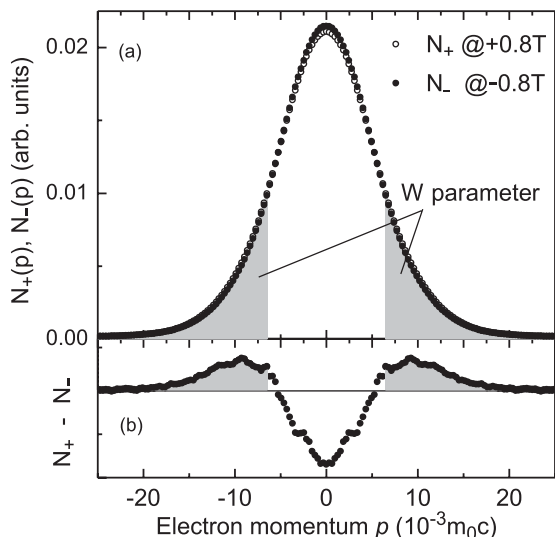


FIG. 2. (a) DBAR spectra obtained for the Fe sample at $B = \pm 0.8$ T and (b) the differential spectrum. These spectra are folded at $p = 0$ to enhance the statistics. Shaded areas denote the windows of the W parameter.

the differences in the band structures of these metals were observed. As shown below, the line-shape parameters exhibit somewhat different field dependences.

Figure 3 shows the so-called W parameter, which is defined as the area intensity in the higher-momentum region as shown in Fig. 2, as a function of the magnetic field. In the case of the Fe sample, the W parameter behaves nearly linearly with the magnetic field, indicating that the annihilation probabilities of

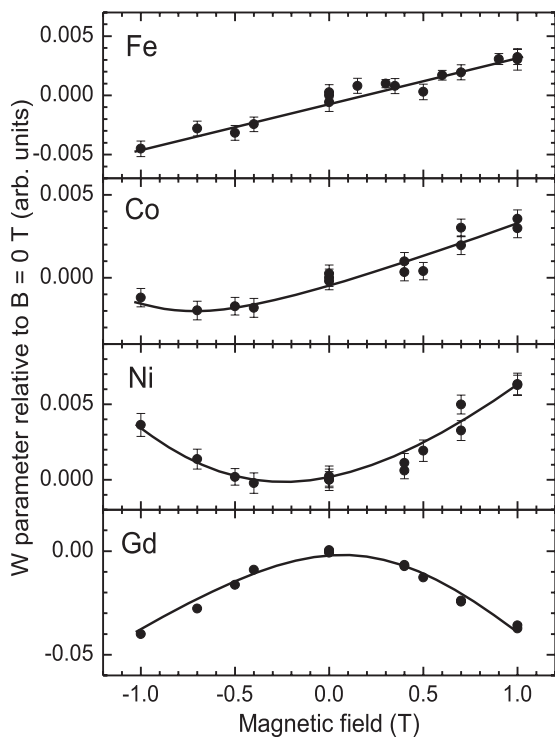


FIG. 3. W parameters as a function of the magnetic field at room temperature obtained for the Fe, Co, Ni, and Gd samples. Solid lines are guides for the eye.

positrons with polarized $3d$ electrons having higher momenta are enhanced under positive fields and reduced under negative fields. For the Co sample, a similar tendency is seen, but the linearity seems to be a little lost under negative fields. In the case of the Ni sample, the deviation from the linear dependence is more pronounced to be somewhat concave-down-parabolic in shape, that is, in both positive and negative fields, the annihilation probabilities of positrons and polarized electrons having higher momenta seem to be enhanced though the amounts are different. As for the the Gd sample, the field dependence is again parabolic, but it is concave up, implying that the annihilation probabilities of positrons with polarized electrons having lower momenta are enhanced under both positive and negative fields. The above results imply that the changes of spectral shapes from those at a zero field reflect the different band structures of these metals.

Figure 4 shows the DBAR differential spectra from a zero field $[N_{+/-}(p) - N_0(p)]$ for the Fe, Co, Ni, and Gd samples at $B = \pm 1$ T. Under a positive field $[N_+(p) - N_0(p)]$, the Fe, Co, and Ni samples exhibit similar features. Under a negative field $[N_-(p) - N_0(p)]$, the spectra of the Fe and Co samples have negative intensities at $|p| \lesssim 3 \times 10^{-3} m_0c$ and $10 \times 10^{-3} \lesssim |p| \lesssim 20 \times 10^{-3} m_0c$, respectively, and positive

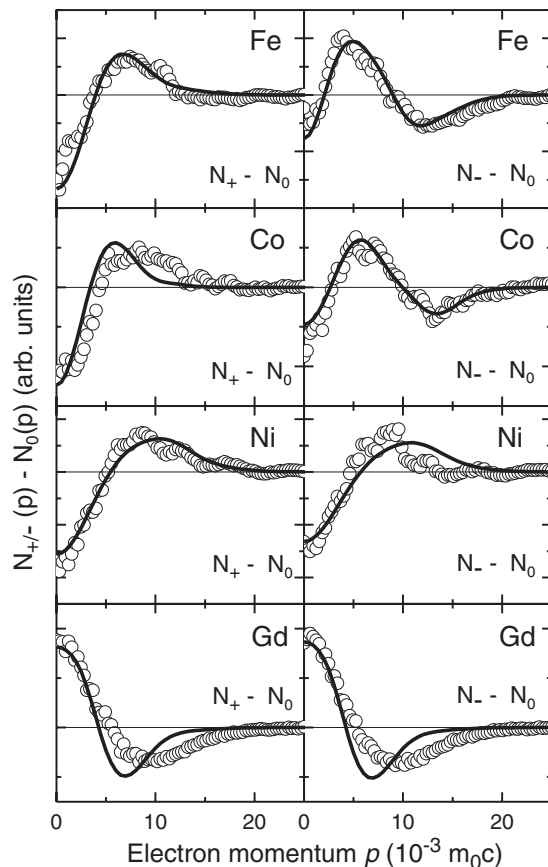


FIG. 4. Differential DBAR spectra between positive or negative and zero fields $[N_{+/-}(p) - N_0(p)]$ for the Fe, Co, Ni, and Gd samples at room temperature ($B = \pm 1$ T). These spectra are folded at $p = 0$ to enhance the statistics. Solid lines denote curves calculated by Berko's method. The amplitudes are adjusted to levels comparable with those in experiments.

intensities at $3 \times 10^{-3} \lesssim |p| \lesssim 10 \times 10^{-3} m_0c$. The spectrum of the Ni sample shows no significant change upon field reversal except for a small change of the intensity. The spectrum of the Gd sample under a positive field exhibits somewhat opposite features to those of the other samples, and its shape is conserved upon field reversal except for a small change in the intensity.

According to the theoretical band structure of Fe,^{16,28–30} the first to fifth majority spin bands are nearly fully occupied, the sixth majority spin band is partially occupied, and the fourth to sixth minority spin bands are empty or only partially occupied. The upper-band electrons have almost *d*-like character while the lower-band electrons have both *sp*-like and *d*-like characters. Hence, the spectrum under a positive field probably reflects the *d*-like characters of the upper majority spin bands while that under a negative field reflects the more *sp*-like characters of the lower minority spin bands.

In the case of Co, the first to tenth majority spin bands are nearly fully occupied, the eleventh and twelfth majority spin bands are partially occupied, and the seventh to twelfth minority spin bands are empty or only partially occupied.³¹ Hence, in Fig. 4, the spectral shape under a positive field probably reflects the *d*-like characters of the upper majority spin bands while that under a negative field reflects the more *sp*-like characters of the lower minority spin bands.

Both the six majority and six minority spin bands of Ni are mostly occupied.^{32,33} Only small amounts of electrons are transferred from the minority to the majority spin bands. Hence, the spectral shapes under both positive and negative fields in Fig. 4 give rise to analogous features, mainly reflecting the fourth to sixth bands having *d*-like character. The slight difference in the intensities upon field reversal is caused by the relatively low occupations of the fifth and sixth minority spin bands.

As for Gd, the *4f* majority spin bands are completely occupied while its minority spin bands are nearly empty.^{34,35} The *5d* majority spin bands are partially occupied while its minority spin bands are empty. Both majority and minority spin bands of the *6s* electrons are nearly occupied. Hence, the field effects are attributed to the *4f* and/or *5d* bands. The annihilation probabilities of *5d* electrons with positrons are much higher than those of inner *4f* shell electrons. The *5d* electrons result in narrower DBAR spectra as compared to the *4f* electrons. Therefore, the field effect on the spectral shape in Fig. 4 likely arises from the *5d* bands. Known as the Ruderman-Kittel-Kasuya-Yoshida (RKKY) interaction, the ferromagnetism of Gd appears due to indirect exchange interactions between *4f* electrons mediated by *5d* electrons. Positrons probably see the polarization of such *5d* electrons.

To elucidate details above, we calculated the differential DBAR spectra for individual bands and the spin-averaged total DBAR spectra. The electron wave functions were obtained from the ABINIT computation³⁶ with the projector-augmented-wave method.³⁷ The initial valence-electron configurations were assumed to be $3s^23p^63d^64s^2$ (Fe), $3s^23p^63d^74s^2$ (Co), $3s^23p^63d^84s^2$ (Ni), and $4f^75s^25p^65d^16s^2$ (Gd). The positron wave function was calculated based on two-component density functional theory. The DBAR spectra were obtained from Eq. (1) with a Gaussian resolution function having a full

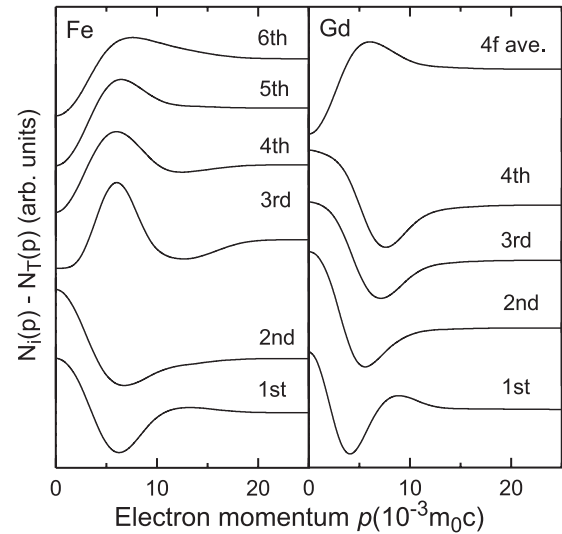


FIG. 5. Differential curves between the *i*th band [$N_i(p)$] and the total DBAR spectra [$N_T(p)$] in the spin-averaged state calculated for Fe and Gd. For Gd, the fourteen *4f* bands are averaged. The amplitudes here are only for comparison.

width at half maximum of 1.4 keV. Since the present samples were polycrystals, the calculated DBAR spectra along the three-momentum axes ([100], [100], and [111] for Fe and Ni and [1100], [1120], and [0001] for Co and Gd) were spherically averaged. The details of the calculations are described elsewhere.³⁸

Figure 5 shows the calculated differential spectra between the spectra of individual bands and the spin-averaged total spectra for Fe and Gd. In Fig. 4, the experimental spectrum of the Fe sample under a positive field exhibits the features of the fourth to sixth bands while under a negative field it exhibits the features of lower bands. The results for the Co and Ni samples may be explained similarly. The experimental spectra of the Gd sample under positive and negative fields in Fig. 4 are similar to those calculated for the first to fourth bands in Fig. 5. (The first and second bands are *6s*-like, and the third and fourth bands are *5d*-like.) The solid lines in Fig. 4 are the differential spectra calculated using Berko's method having the occupations of individual bands.^{6,19} (The amplitudes of the calculated spectra are adjusted to levels comparable with those in experiments.) Although the calculated differential spectra are not fully compatible with the experimental spectra, their agreement is generally good.

In a previous work, we found that the strength of the field-reversal asymmetry of the DBAR spectra for Fe, Co, and Ni is approximately proportional to their magnetization. In these metals, the annihilation probabilities between positrons and valence (*3d4s*) electrons are comparable because of their close electron densities. Hence, the field-reversal asymmetry observed for these metals is approximately proportional to the averaged spin polarizations of the valence bands, i.e., magnetizations.

Similar discussion may be allowed for Gd, Tb, and Dy. The field-reversal asymmetry observed for the Tb and Dy samples was much smaller ($<1/7$) as compared to the Gd sample. As discussed above, in these metals, the field effect on the DBAR spectra is caused by polarized *5d* electrons. Therefore, the

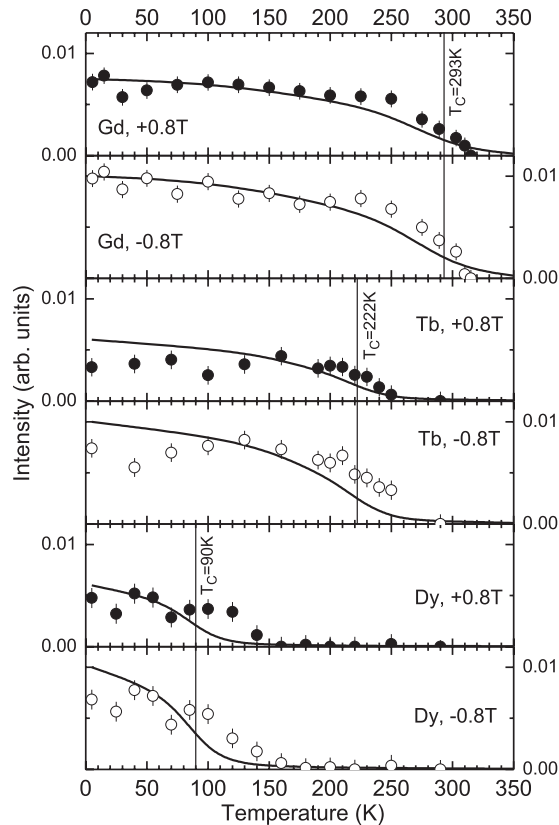


FIG. 6. Area intensities of the differential DBAR spectra relative to those at the highest temperatures obtained for the Gd, Tb, and Dy samples at $B = 0.8$ T as a function of temperature. The Curie temperatures (T_C) of the ferromagnetic-phase transition are indicated. Solid lines are the calculated temperature dependences based on the Weiss theory.

suppressed field-reversal asymmetry of the Tb and Dy samples implies much lower polarizations of their $5d$ bands compared to that of Gd.

B. Temperature dependence

Under a magnetic field, the DBAR spectra of the Fe, Co, and Ni samples showed no apparent temperature dependences below 315 K while the field effects on the DBAR spectra for the rare-earth samples increased upon cooling. Figure 6

shows the temperature dependences of the intensities of the DBAR spectra relative to those at the maximum temperature $T_M = \int_{-\infty}^{+\infty} |N_{T=T}(p) - N_{T=T_M}(p)| dp$, obtained for the Gd, Tb, and Dy samples at $B = \pm 0.8$ T. The intensities under a negative field are greater than those under a positive field. This is consistent with the results shown in Fig. 4. The critical temperatures at which the field effects vanish seem to be in agreement with the Curie temperatures (T_C) associated with the ferromagnetic-phase transitions of these metals (Gd: 293 K, Tb: 222 K, and Dy: 90 K). The absence of temperature dependences for the Fe, Co, and Ni samples is explained by their high Curie temperatures.

The temperature dependence of magnetization (M) is given by the Weiss equation

$$\frac{M}{M_0} = B_J \left[\frac{g_J \mu_B J (B + \lambda M)}{k_B T} \right], \quad (6)$$

where M_0 is the magnetization at $T = 0$ K, J is the total angular momentum (Gd: $7/2$, Tb: 6, and Dy: $15/2$), g_J is the Landé's g factor (Gd: 2, Tb: 1.5, and Dy: 1.33), μ_B is the Bohr magneton, B_J is the Brillouin function, k_B is the Boltzmann constant, and λ is the molecular-field constant ($3k_B T_C$)/ $[N g_J^2 \mu_B^2 J(J+1)]$. Solid lines M/M_0 are calculated assuming that the DBAR intensity is proportional to the magnetization. (The amplitudes are adjusted to levels comparable with those in experiments.) The experimental temperature dependences are qualitatively reproduced. Thus, the above results demonstrate that the polarizations of the $5d$ bands and hence the magnetizations are lost upon heating.

V. CONCLUSION

In conclusion, we examined the magnetic-field and temperature dependences of the DBAR spectra for $3d$ and $4f$ ferromagnets. The different field dependences observed for Fe, Co, Ni, and Gd were explained by considering their different band structures. We found that the field effects on DBAR spectra for Gd, Tb, and Dy disappear above ferromagnetic-phase-transition temperatures. These results suggest that spin-polarized positron annihilation spectroscopy can be used in characterizing the polarized electrons of ferromagnets and also in spin-related phenomena. A highly spin-polarized-positron beam is required for performing such advanced research.

*kawasuso.atsuo@jaea.go.jp

¹S. S. Hanna and R. S. Preston, *Phys. Rev.* **106**, 1363 (1957).

²S. S. Hanna and R. S. Preston, *Phys. Rev.* **109**, 716 (1958).

³P. E. Mijnarends and L. Hambro, *Phys. Lett.* **10**, 272 (1964).

⁴P. E. Mijnarends, *Physica (Amsterdam)* **63**, 248 (1973).

⁵S. Berko and J. Zuckerman, *Phys. Rev. Lett.* **13**, 339 (1964).

⁶S. Berko, in *Positron Annihilation*, edited by A. T. Stewart and L. O. Roellig (Academic Press, New York, 1967), p. 61.

⁷S. Berko and A. P. Mills, *J. Phys., Colloq.* **32**, C1 (1971).

⁸C. Hohenemser, J. M. Weingart, and S. Berko, *Phys. Lett. A* **28**, 41 (1968).

⁹T. W. Mihalisin and R. D. Parks, *Phys. Lett.* **21**, 610 (1966).

¹⁰T. W. Mihalisin and R. D. Parks, *Phys. Rev. Lett.* **18**, 210 (1967).

¹¹T. W. Mihalisin and R. D. Parks, *Solid State Commun.* **7**, 33 (1969).

¹²N. Shiotani, T. Okada, H. Sekizawa, T. Mizoguchi, and T. Karasawa, *J. Phys. Soc. Jpn.* **35**, 456 (1973).

¹³M. Šob, S. Szuszkiewicz, and M. Szuszkiewicz, *Phys. Status Solidi B* **123**, 649 (1984).

¹⁴T. Jarborg, A. A. Manuel, Y. Mathys, M. Peter, A. K. Singh, and E. Walker, *J. Magn. Magn. Mater.* **54–57**, 1023 (1986).

¹⁵S. Szuszkiewicz, M. Šob, and M. Szuszkiewicz, *J. Magn. Magn. Mater.* **62**, 202 (1986).

- ¹⁶P. Genoud, A. K. Singh, A. A. Manuel, T. Jarlborg, E. Walker, M. Peter, and M. Welle, *J. Phys. F* **18**, 1933 (1988).
- ¹⁷P. Genoud, A. A. Manuel, E. Walker, and M. Peter, *J. Phys.: Condens. Matter* **3**, 4201 (1991).
- ¹⁸H. Kondo, T. Kubota, H. Nakashima, T. Kawano, and S. Tanigawa, *J. Phys.: Condens. Matter* **4**, 4595 (1992).
- ¹⁹A. Kawasuso, M. Maekawa, Y. Fukaya, A. Yabuuchi, and I. Mochizuki, *Phys. Rev. B* **83**, 100406(R) (2011).
- ²⁰P. W. Zitzewitz, J. C. van House, A. Rich, and D. W. Gidley, *Phys. Rev. Lett.* **43**, 1281 (1979).
- ²¹D. W. Gidley, A. R. Köymen, and T. W. Capelhart, *Phys. Rev. Lett.* **49**, 1779 (1982).
- ²²A. Kawasuso and M. Maekawa, *Appl. Surf. Sci.* **255**, 108 (2008).
- ²³P. G. Coleman and A. Kallis, *J. Phys.: Conf. Ser.* **262**, 012016 (2011).
- ²⁴M. Alatalo, M. Puska, and R. M. Nieminen, *J. Phys.: Condens. Matter* **5**, L307 (1993).
- ²⁵E. Boroński and R. M. Nieminen, *Phys. Rev. B* **34**, 3820 (1986).
- ²⁶Y. Nagai, Y. Nagashima, J. Kim, Y. Itoh, and T. Hyodo, *Nucl. Instrum. Methods Phys. Res., Sect. B* **171**, 199 (2000).
- ²⁷J. Major, in *Positron Beams and Their Applications*, edited by P. Coleman (World Scientific, Singapore, 1999), p. 259.
- ²⁸S. Wakoh and J. Yamashita, *J. Phys. Soc. Jpn.* **21**, 1712 (1966).
- ²⁹J. Callaway and C. S. Wang, *Phys. Rev. B* **16**, 2095 (1977).
- ³⁰Y. Kubo and S. Asano, *Phys. Rev. B* **42**, 4431 (1990).
- ³¹M. Matsumoto, K. Tomimoto, and S. Wakoh, *J. Phys. Soc. Jpn.* **62**, 2734 (1993).
- ³²S. Wakoh, *J. Phys. Soc. Jpn.* **20**, 1894 (1965).
- ³³Y. Kakutani, Y. Kubo, A. Koizumi, N. Sakai, B. L. Ahuja, and B. K. Sharma, *J. Phys. Soc. Jpn.* **72**, 599 (2003).
- ³⁴J. Sticht and J. Kübler, *Solid State Commun.* **53**, 529 (1985).
- ³⁵H. Yamagami, *J. Phys. Soc. Jpn.* **67**, 3176 (1998).
- ³⁶X. Gonze, J.-M. Beuken, R. Caracas, F. Detraux, M. Fuchs, G.-M. Rignanese, L. Sindic, M. Verstraete, G. Zerah, F. Jollet, M. Torrent, A. Roy, M. Mikami, Ph. Ghosez, J.-Y. Raty, and D.C. Allan, *Comput. Mater. Sci.* **25**, 478 (2002).
- ³⁷P. E. Blöchl, *Phys. Rev. B* **50**, 17953 (1994).
- ³⁸A. Kawasuso, M. Maekawa, and K. Betsuyaku, *J. Phys.: Conf. Ser.* **225**, 012027 (2010).